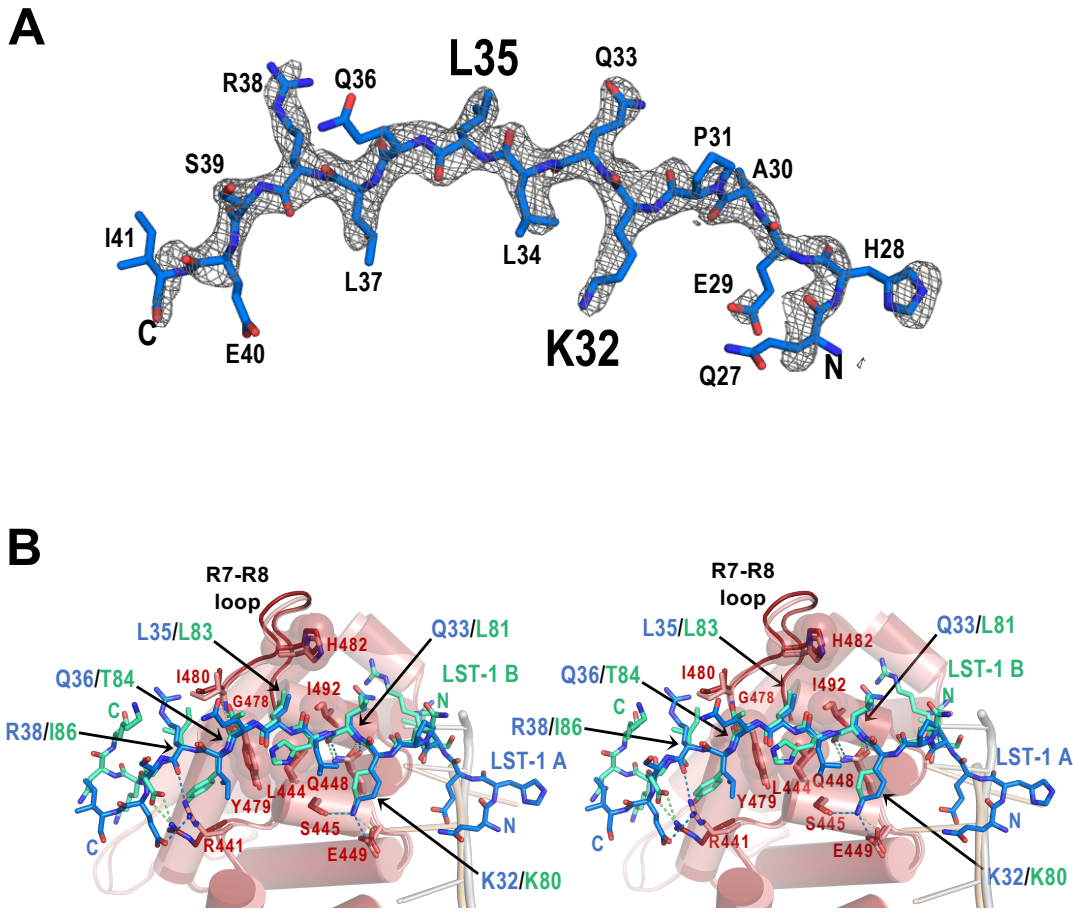

Crystal structures of complexes of FBF-2, LST-1 A or B, and cFBE RNA reveal distinct paths of LST-1 peptides on the surface of FBF-2. (**A**) F_o-F_c omit map for the LST-1 A peptide. An F_o-F_c omit map for the LST-1 A peptide, contoured at 3 σ, is superimposed on a stick model of the peptide. (B) Stereo image of the interaction of FBF-2 with LST-1 A or B in complexes with cFBE RNA. The LST-1 peptides are shown as stick models, and cFBE RNAs are shown as cartoons. FBF-2 residues that interact with LST-1 are displayed as stick models. Side chains that form a hydrophobic pocket for L35/L83 are shown with transparent spheres. Hydrogen bond and salt bridge interactions are indicated with dashed lines (LST-1 A, blue; LST-1 B, green).

Figure S2

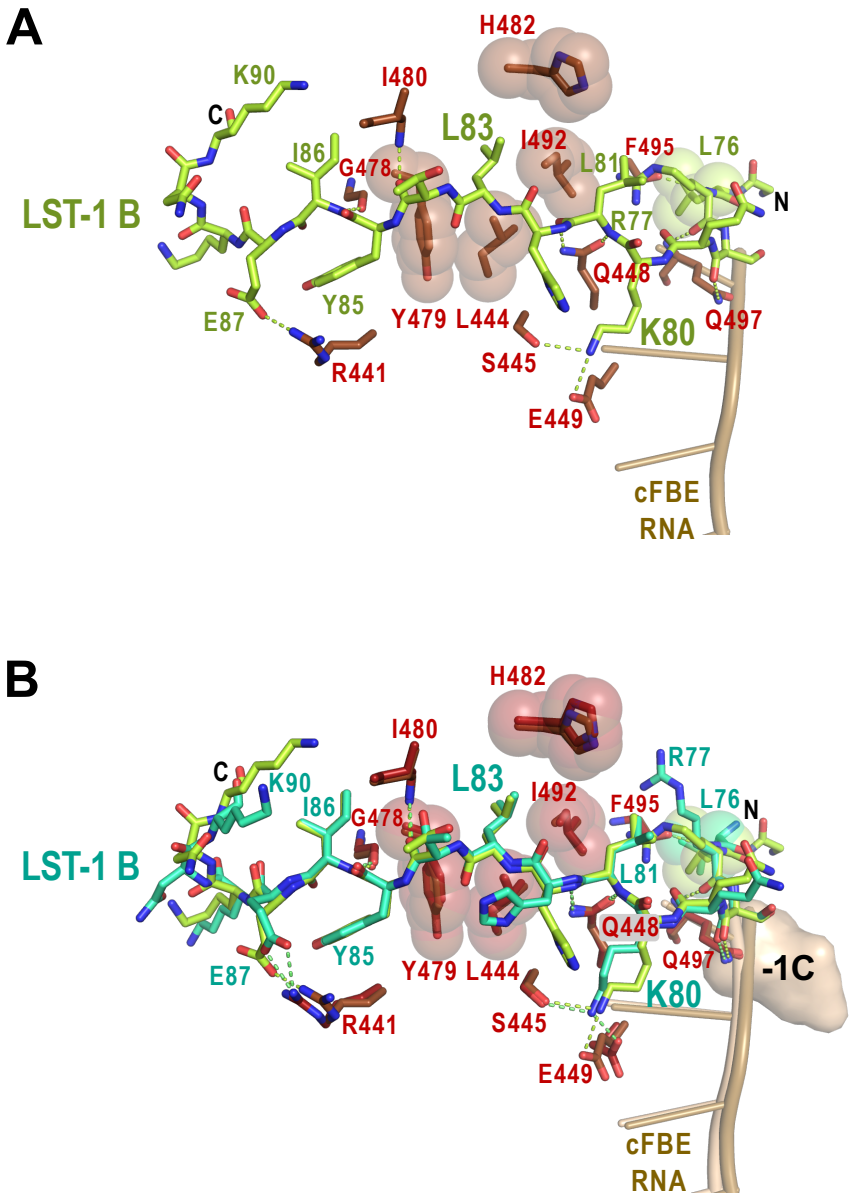

FBF-2 interacts with LST-1 B peptide similarly in two independent complexes in an asymmetric unit. (**A**) FBF-2 interactions with LST-1 B peptide are shown for the second of two complexes in the asymmetric unit (PDB ID 6PUN, FBF-2 chain B). FBF-2 residues (brown) that interact with LST-1 (light green) are displayed as stick models. L76 and side chains that form a hydrophobic pocket for L83 are shown with transparent spheres. Hydrogen bond and salt bridge interactions are indicated with dashed lines. (**B**) Superposition of the two FBF-2/LST-1 B/cFBE RNA complexes.

Figure S3

A

```
LST-1 A (19-50) STIAYSKSQHEAPKQLLQLRSEIKPLIPLNQP
LST-1 B (67-98) SSSPQQRSGLRSQKLHLTYIEKNKRVRAMIPQ
LST-1 B  mutN   SSSPQQRSGHEAPKLHLTYIEKNKRVRAMIPQ
LST-1 B  mutC   SSSPQQRSGLRSQKLHLTLRSENKRVRAMIPQ
LST-1 B  Y85L   SSSPQQRSGLRSQKLHLTLIEKNKRVRAMIPQ
```

B

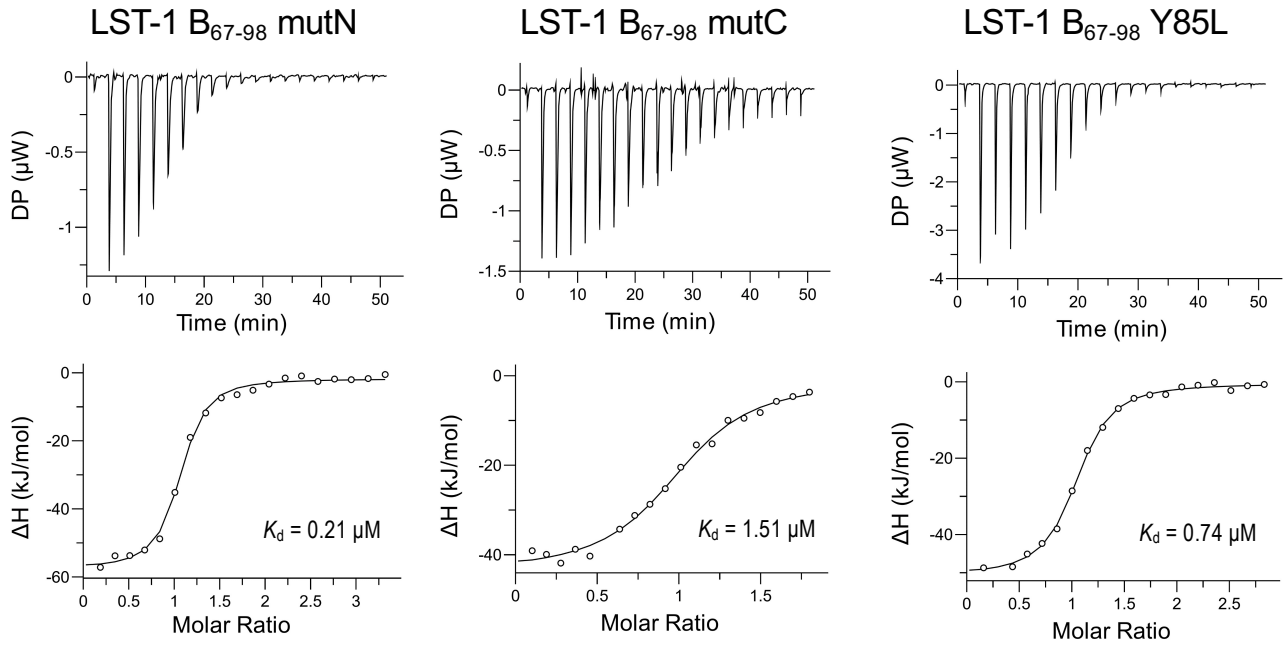

Substitution of residues flanking the KxxL motif in LST-1 B decreases its affinity for FBF-2. (**A**) The sequences of LST-1 A and LST-1 B peptide variants used for calorimetry are shown with the KxxL motifs boxed. Substitutions in LST-1 B peptides are blue. (**B**) Substitution of residues flanking the KxxL motif in LST-1 B weaken affinity for FBF-2. Representative isothermal titration calorimetry thermograms (top) and corresponding titration curve-fitting graphs (bottom) are shown. K_d for the experiment shown is indicated (N=1). Thermodynamic parameters are summarized in Table 1.

Figure S4

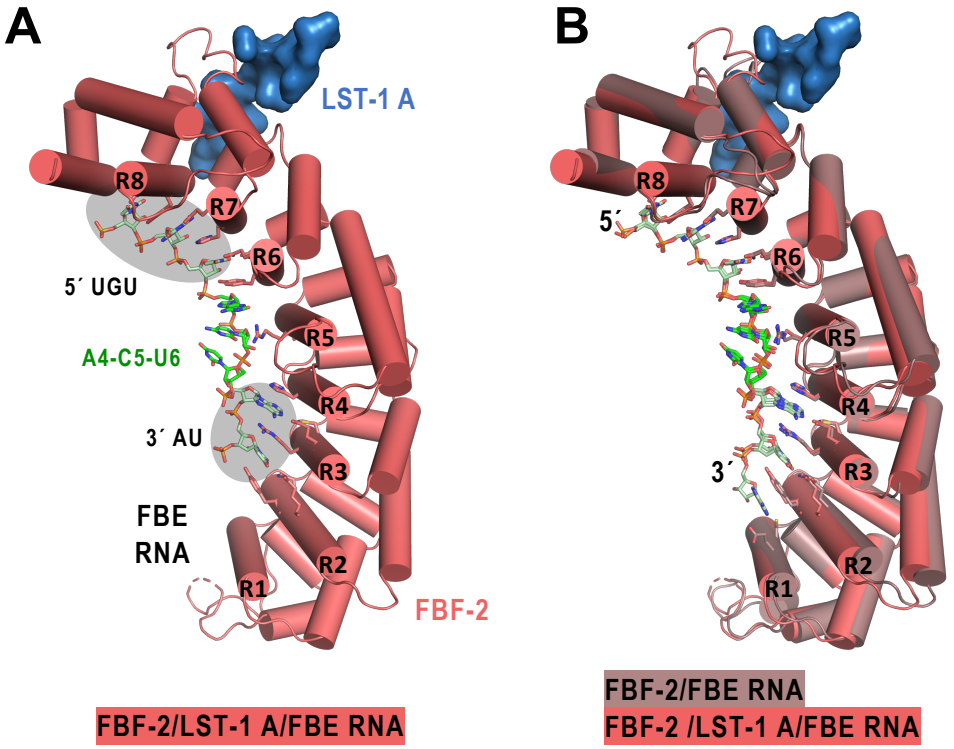

FBF-2 in complex with LST-1 A peptide interacts with a 9-nt FBE RNA using the two-handed RNA recognition mode. (**A**) FBF-2 recognizes a consensus FBE RNA using the two-handed recognition mode where FBF-2 recognizes the 5´-UGU and AU-3´ elements (grey ovals). A crystal structure of FBF-2 and LST-1 A peptide in complex with consensus FBE RNA (5´-UGUACUAUA-3´) is shown. The RNA-binding helices of FBF-2 repeats 1-8 (R1-R8) are labeled. (**B**) FBF-2 curvature is similar in complexes with FBE RNA with or without LST-1 A. The structures of FBF-2 complexes are shown from panel A and Figure 4A. Residues 313-567 of FBF-2 were aligned (RMSD 0.43 Å over 1597 atoms).

Figure S5

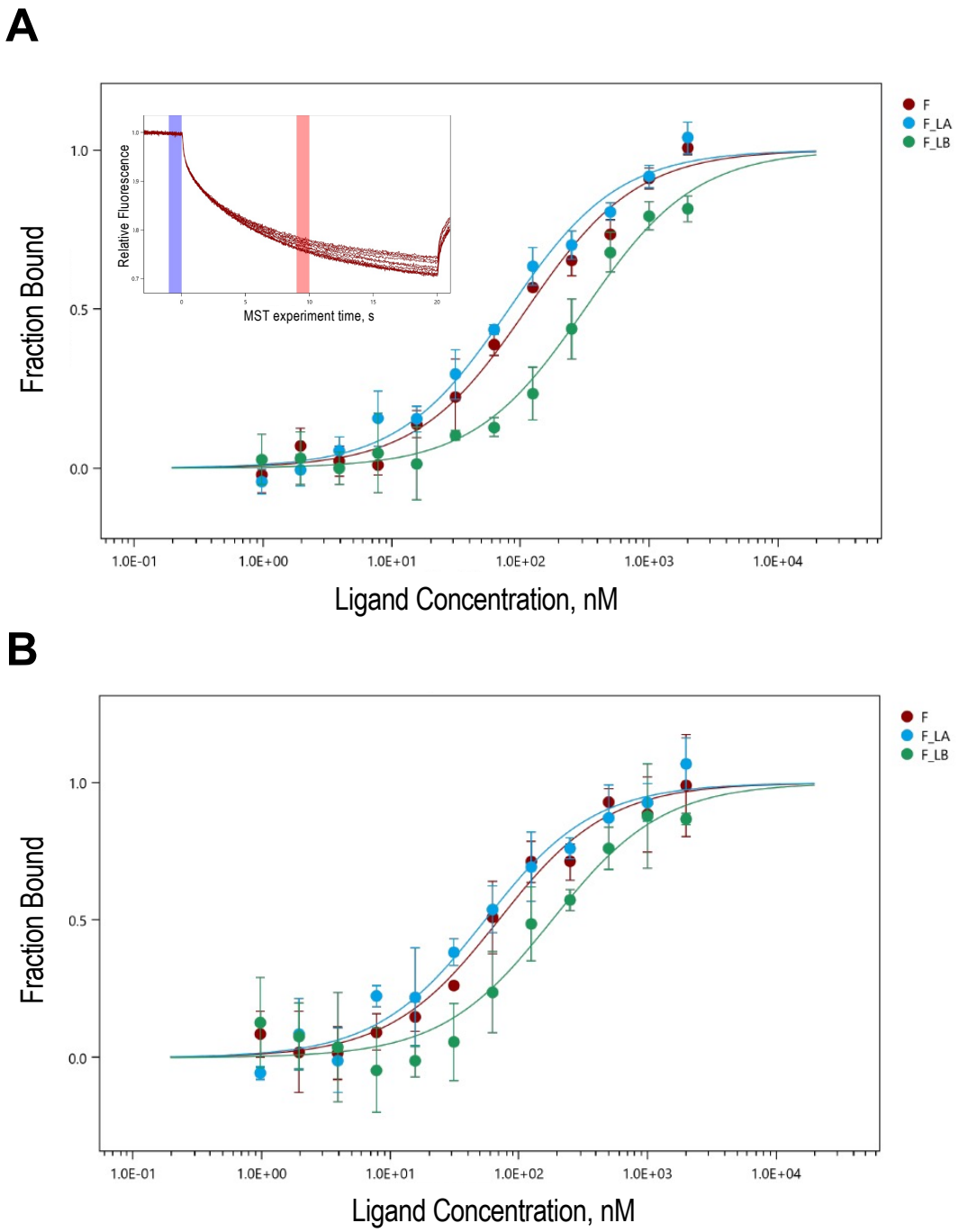

LST-1 B weakens the affinity of FBF-2 for *gld-1* FBEa and cFBE RNAs, but the presence of LST-1 A makes no significant change in affinity. (**A**) MST analysis of binding to 3´-Cy5 labeled *gld-1* FBEa RNA by FBF-2 alone (F, red) or in the presence of LST-1 A (F_LA, blue) or LST-1 B (F_LB, green). Inset: MST traces from one measurement of FBF-2 binding to *gld-1* FBEa RNA. The blue bar indicates F_{cold} at 0 sec before the IR-laser was turned on, and the red bar indicates F_{hot} at 10 s after the laser was turned on. Normalized fluorescence F_{norm} is defined as F_{hot}/F_{cold}. (**B**) MST analysis of binding to 3´-Cy5 labeled cFBE RNA by FBF-2 alone (red) or in the presence of LST-1 A (blue) or LST-1 B (green). The mean fraction of bound RNA calculated from the change in normalized fluorescence from three independently pipetted replicates is plotted versus the concentration of FBF-2. The standard deviations for each measurement are shown as error bars, and the best fit curve to a 1:1 binding model is superimposed.